

Delamination Analysis of Carbon Fiber Composites Under Dynamic Loads Using Acoustic Emission

X. K. Li · P. F. Liu

Submitted: 2 October 2015 / Published online: 13 January 2016
© ASM International 2016

Abstract Non-destructive test technique for monitoring delamination failure under complicated loads and environments is still not mature until now. The purpose of this research is to study mixed-mode delamination properties of carbon fiber/epoxy composite laminates under dynamic loads using acoustic emission (AE). Different lay-up specimens with initial intralaminar and interlaminar defects are tested. Two loading modes including single-leg and over-leg three-point bending are applied under dynamic and quasi-static loads. By analyzing the load–displacement curves and the responses of AE characteristic parameters including amplitude and count, effects of the loading speed, loading mode, and lay-up pattern on the delamination initiation and propagation behaviors are studied. Besides, different failure mechanisms are observed by scanning electron microscope. AE results show that the loading speed and mode affect the delamination behaviors of composites distinctly.

Keywords Dynamic loading · Delamination · Acoustic emission · Carbon fiber/epoxy composite laminates

Introduction

Compared with metal materials, complicated failure mechanisms are distinct features of carbon fiber composites which generally include intralaminar fiber breakage,

matrix cracking, fiber/matrix interface debonding, and interlaminar delamination [1, 2]. In particular, delamination decreases the stiffness, strength, and integrity of composite structures largely. Furthermore, complicated load modes including typical dynamic loads are demonstrated to affect the mechanical properties largely, especially delamination failure. For example, many composite structures such as airplanes and wind turbine blades often experience these loads. Therefore, it is essential to understand how the load speed degrades the mechanical properties of composites.

In order to gain deep insight into the delamination properties of composites, advanced experimental approaches are urgently needed. Currently, acoustic emission (AE) has become an efficient technique for dynamically monitoring the damage evolution behaviors of composites [3]. Various failure mechanisms above were identified by analyzing the responses of AE characteristic parameters such as the amplitude, energy, and duration [4]. Fotouhi et al. [5] used the AE energy and count rate distribution to determine the critical force at the delamination onset for glass/epoxy composites under three-point bending test. Scholey et al. [6] performed quantitative measurement on the AE events including the amplitude and angular variation due to matrix cracking and delamination under quasi-static loads. Silversides et al. [7] used the AE cumulative energy to determine the delamination onset and propagation in carbon fiber composites under quasi-static and fatigue loads. Liu et al. [8] used the AE amplitude and energy to study the effects of the lay-up pattern and initial defect on the delamination behaviors of carbon fiber/epoxy composites. However, until now there was little research on the delamination behaviors of composites under dynamic loads using AE.

X. K. Li · P. F. Liu (✉)
Institute of Chemical Machinery and Process Equipment,
Zhejiang University, Hangzhou 310027, China
e-mail: pfliu@zju.edu.cn

In this paper, three-point bending experiment and AE test on carbon fiber/epoxy composite laminates with initial intralaminar and interlaminar defects are performed under quasi-static and dynamic loads. By analyzing the responses of the AE amplitude and count rate, the effects of the loading speed, loading mode, and lay-up pattern on the delamination behaviors of composites are comparatively studied. This work provides a fundamental and technical support for revealing the delamination behaviors of composites under dynamic loads.

Material Specimens

Two lay-up patterns of T700/BA9916 composite laminates including $[0^\circ]_{16} // [0^\circ]_{16}$ and $[0^\circ/90^\circ]_{4s} // [0^\circ/90^\circ]_{4s}$ are used for AE test. Material and geometry parameters are listed in Tables 1 and 2, respectively. Each specimen includes 32 plies, and the fiber volume fraction is 61%. A Teflon film is

inserted at the middle plane of specimens to make an initial delamination crack.

Three-Point Bending Testing and AE Monitoring

Currently, single-leg bending (SLB) has become a common method to study the delamination behaviors of composites. Based on the SLB, Szekrenyes and Uj [9] further proposed the over-leg bending (OLB) loading mode. In this research, these two loading modes are comparatively used, as shown in Fig. 1. Three-point bending test is performed using a UTM5000 electronic test machine. Loading speed under quasi-static and dynamic loads is 2 and 100 mm/min, respectively. A 48-channel AE equipment is used, and two AE sensors are placed on two ends of composite specimens. The AE equipment is composed of a transducer, a 2/4/6-AST preamplifier, and a PAC Samos-48 AE apparatus, as shown in Fig. 2. AE signals are detected by sensors and enhanced by the preamplifier which

Table 1 Elastic parameters for T700/BA9916 composites

E_{11} (GPa)	E_{33} (GPa)	E_{33} (GPa)	G_{12} (GPa)	G_{13} (GPa)	ν_{12}	ν_{13}
116	8.9	8.9	4.15	4.15	0.27	0.27

E and G the Young’s modulus and shear modulus, respectively

Table 2 Geometry sizes and lay-up patterns for two composite specimens

Number	Length × width × thickness, mm	Initial crack length, mm	Truncation length, mm	Lay-up patterns
①	150 × 20 × 4.8	50	25	$[0^\circ]_{16} // [0^\circ]_{16}$
②	150 × 20 × 4.8	50	25	$[0/90]_{4s} // [0/90]_{4s}$

subscript s symmetry; // delaminated interface

Fig. 1 Composite specimens under (a) SLB and (b) OLB. a is the crack length, L is the half span length, b is the truncation length, $h/2$ is a half of the specimen thickness, and P is the external force

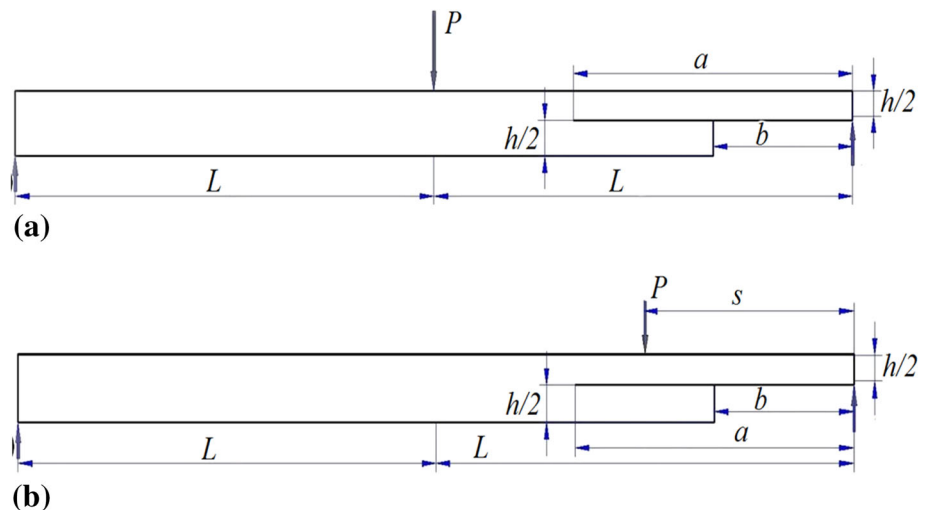


Fig. 2 Schematic description of (a) AE test system and (b) delamination test

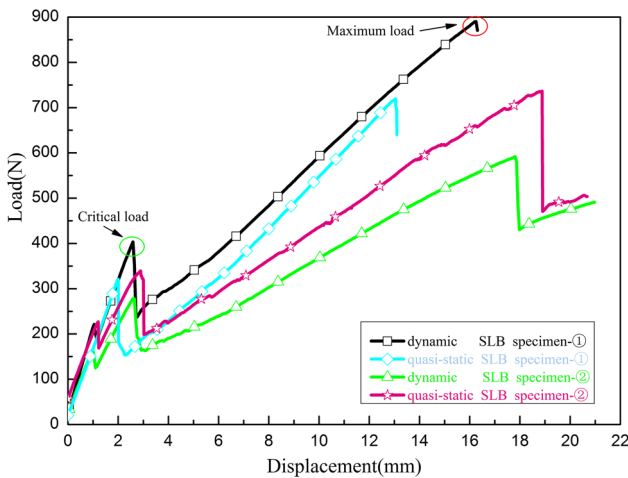
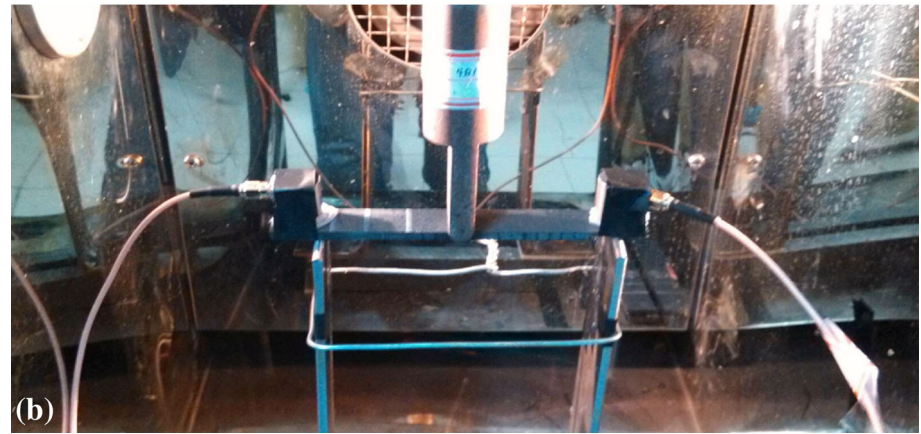
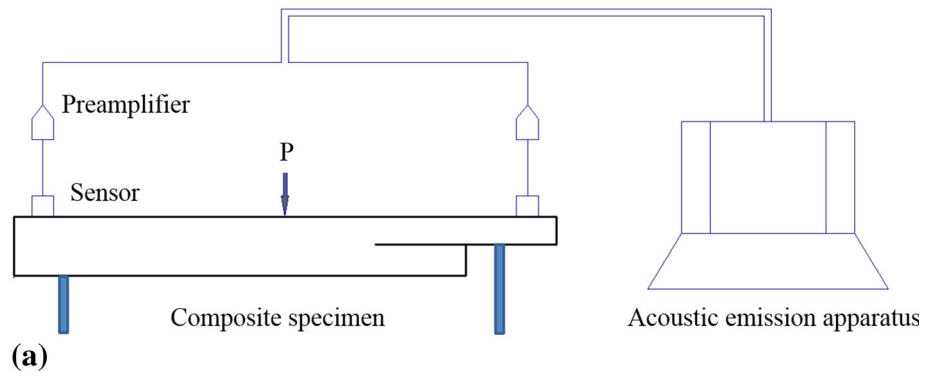


Fig. 3 Load–displacement curves for the specimens under dynamic and quasi-static SLB

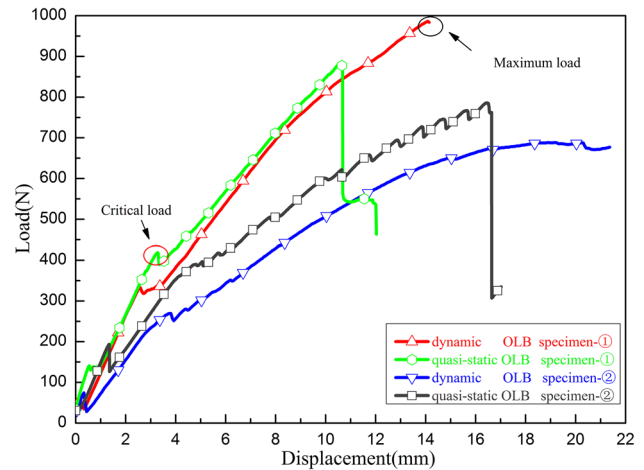


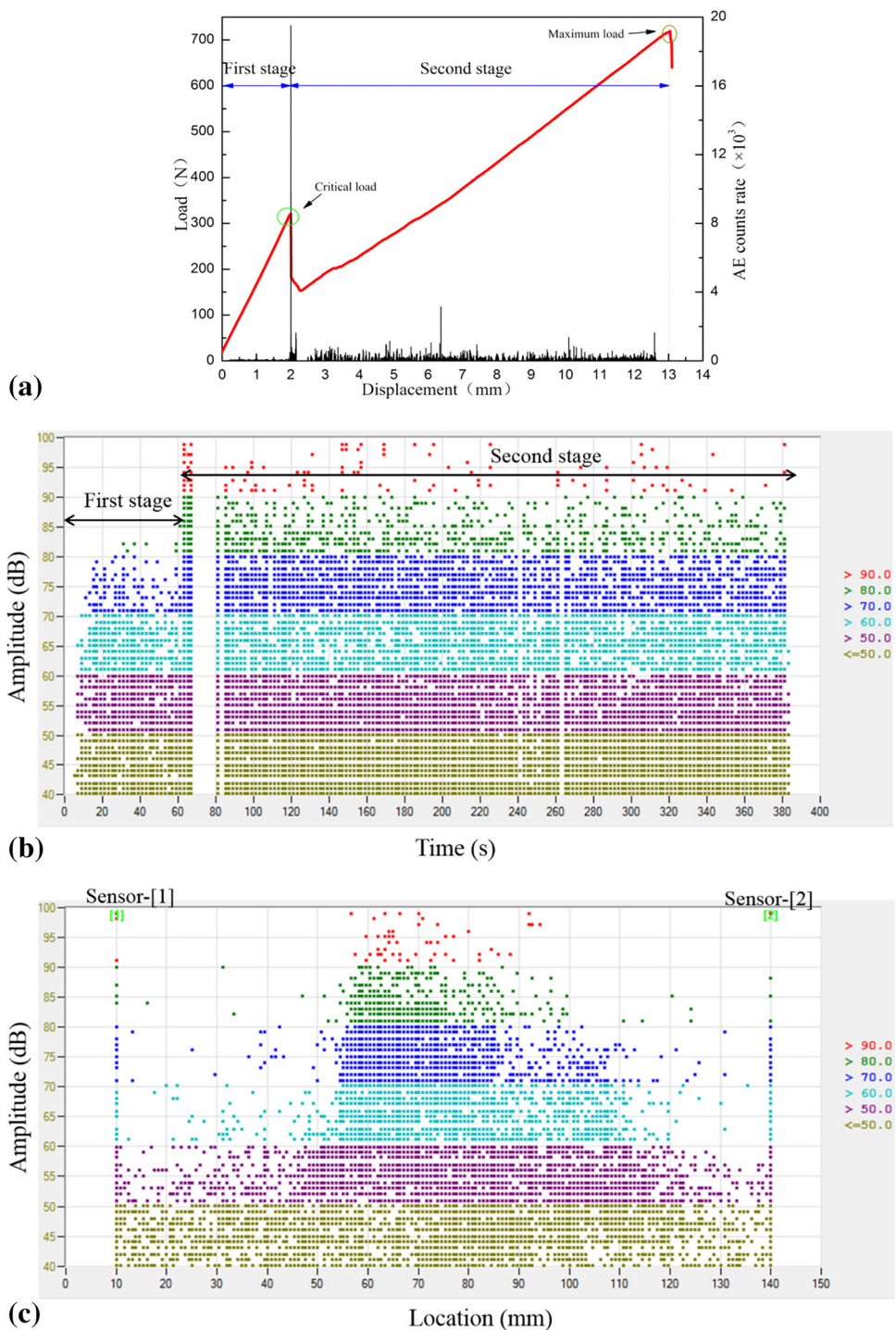
Fig. 4 Load–displacement curves for the specimens under dynamic and quasi-static OLB

employs enlarging circuits with a frequency range from 50 kHz to 2 MHz. The gain selector of the preamplifier is set to 40 dB in order to filter the environmental noise. Timing parameters are as follows: peak definition time (PDT) = 50 μ s, hit definition time (HDT) = 200 μ s, and hit lockout time (HLT) = 300 μ s. The responses of AE parameters including the count rate and amplitude are recorded during the test.

Mechanical Properties of Composite Specimens

Figure 3 shows the load–displacement curves for the specimens under dynamic and quasi-static SLB. Figure 4 shows the load–displacement curves for the specimens under dynamic and quasi-static OLB. In Figs. 3 and 4, each curve has two local peak points. The first peak point

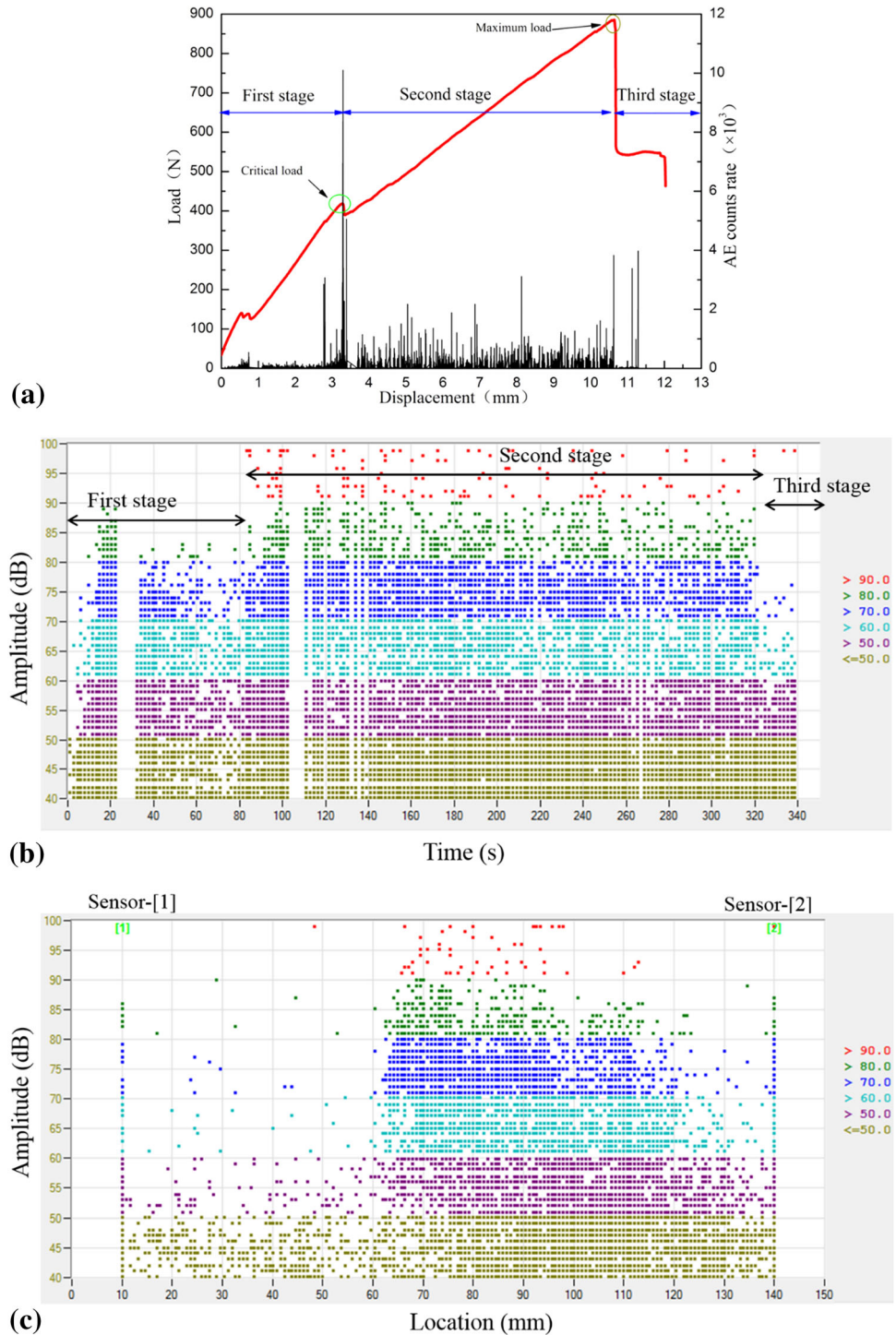
Fig. 5 (a) Load/count rate-displacement distributions, (b) amplitude-time distribution and (c) amplitude-location distribution for the $[0^\circ_{16}/0^\circ_{16}]$ specimen under quasi-static SLB



corresponds to the critical value for the delamination initiation and the second peak point represents the collapse of structures. Under both SLB and OLB for the $[0^\circ_{16}/0^\circ_{16}]$ specimen, the maximum load under dynamic loads is larger than that under quasi-static loads. However, the $[0^\circ/90^\circ]_{4s}/[0^\circ/90^\circ]_{4s}$ specimen leads to opposite

results, indicating the loading speed has different effects for different lay-up specimens. Besides, the curve of the $[0^\circ_{16}/0^\circ_{16}]$ specimen is well above that of the $[0^\circ/90^\circ]_{4s}/[0^\circ/90^\circ]_{4s}$ specimen under dynamic loads, indicating the load-bearing abilities for the $[0^\circ_{16}/0^\circ_{16}]$ specimen are stronger than those for the $[0^\circ/90^\circ]_{4s}/[0^\circ/90^\circ]_{4s}$ specimen

Fig. 6 (a) Load/count rate-displacement distributions, (b) amplitude-time distribution, and (c) amplitude-location distribution for the $[0^\circ_{16}/0^\circ_{16}]$ specimen under quasi-static OLB

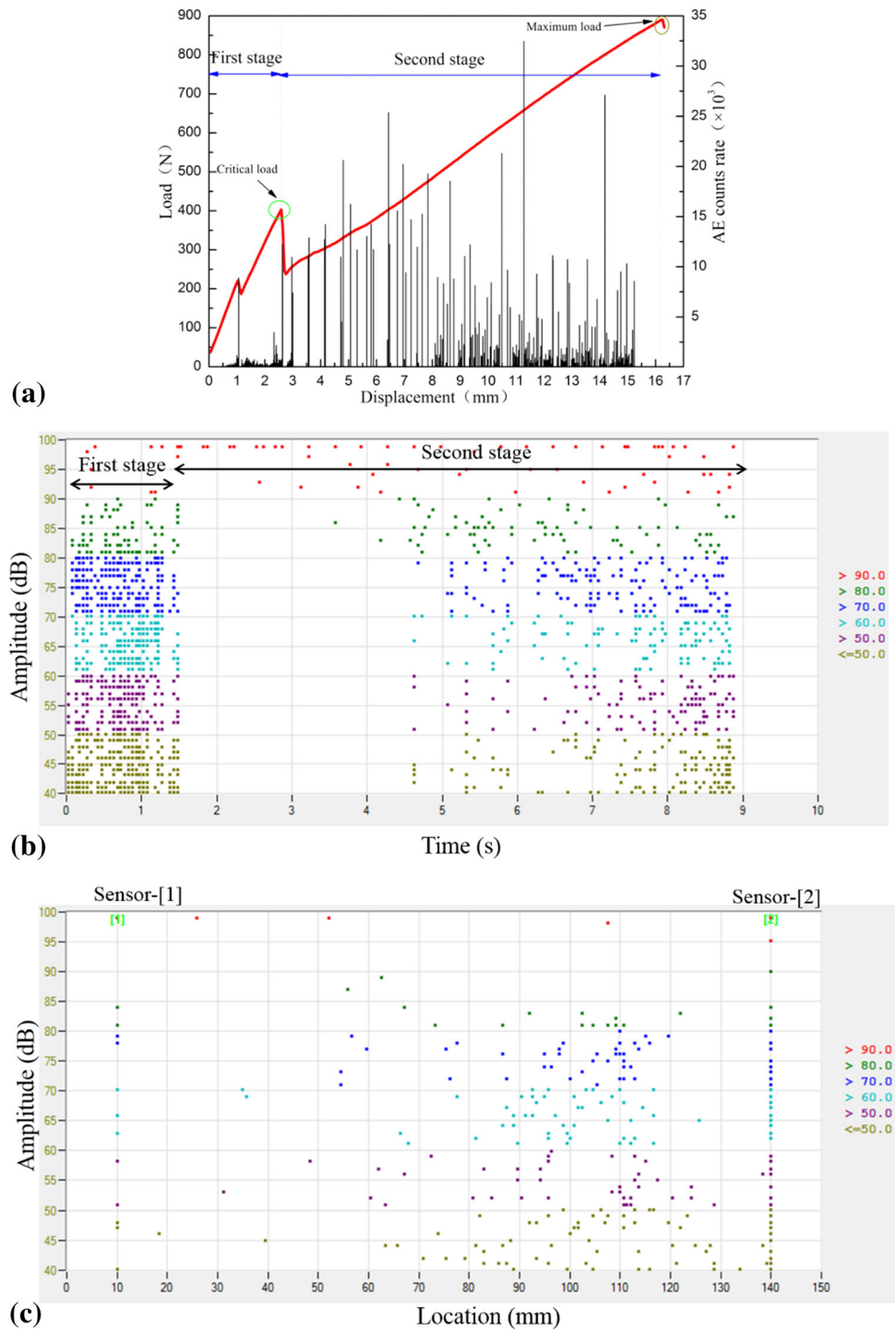


under dynamic loads. Finally, the delamination crack for the $[0^\circ/90^\circ]_{4s}/[0^\circ/90^\circ]_{4s}$ specimen propagates more quickly than that for the $[0^\circ_{16}/0^\circ_{16}]$ specimen, indicating the dynamic delamination resistance for the $[0^\circ_{16}/0^\circ_{16}]$ specimen is stronger than that for the $[0^\circ/90^\circ]_{4s}/[0^\circ/90^\circ]_{4s}$ specimen.

Delamination Behaviors of Composite Specimens Under Quasi-static Loads

Figure 5 shows the load/count rate-displacement distributions, the amplitude-time distribution, and the amplitude-location distribution for the $[0^\circ_{16}/0^\circ_{16}]$ specimen under

Fig. 7 (a) Load/count rate-displacement distributions, (b) amplitude-time distribution, and (c) amplitude-location distribution for the $[0^\circ_{16}/0^\circ_{16}]$ specimen under dynamic SLB



quasi-static SLB. As shown in Fig. 5a, an abrupt change of load corresponds to the count rate peak, which means the AE count rate is high, while the load decreases steeply. The failure process can be divided into three stages, as shown in Fig. 5a and b. The first stage corresponds to the elastic deformation where the strain energy is less than the critical value at the crack tip and the initial crack does not

propagate [5, 10]. The slope of the load–displacement curve is high and approximately linear when the load reaches the critical value rapidly. During the elastic deformation, low AE count rate is mixed with 40–60 dB matrix cracking, 50–70 dB interface debonding, 60–80 dB delamination, and few 80–100 dB fiber breakage signals [11–13]. The second stage corresponds to the delamination

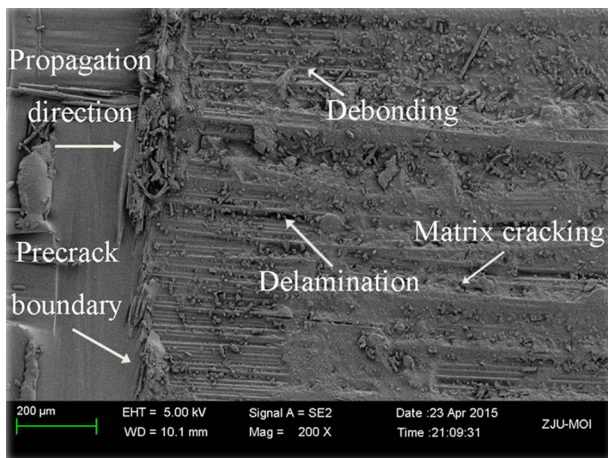


Fig. 8 SEM observation of failure mechanisms at the crack tip for the $[0^\circ]_{16}/[0^\circ]_{16}$ specimen under dynamic SLB

crack propagation when the strain energy release rate exceeds the critical value [10]. After the delamination crack starts to propagate, the load decreases abruptly with the increase of count rate. Because of the stiffness degradation due to delamination [4], the slope of the load–displacement curve is smaller than that at the first stage [14]. Due to various damage mechanisms at the crack tip, there are signals with a wide range of amplitudes represented by matrix cracking, interface debonding, interlaminar delamination, and fiber breakage. In the third stage, the specimen collapses after reaching the maximum load. According to the amplitude–location distribution shown in Fig. 5c, there are two sites with dense amplitude signals: the loading end and the initial crack tip. Due to the crack propagation and fiber breakage at the loading end, 80–100 dB signals mainly gather at the 55–85 mm location. Besides, there are also some high-decibel signals at the 95–110 mm location because of the initial intralaminar and interlaminar defects. In addition, there are 40–60 dB matrix cracking, 50–70 dB interface debonding signals at the 10–55 mm location due to the bending stress. By identifying the location with high-amplitude signals, the delamination crack propagates to approximately the 55 mm location.

Figure 6 shows the load/count rate–displacement distributions, the amplitude–time distribution, and the amplitude–location distribution for the $[0^\circ]_{16}/[0^\circ]_{16}$ specimen under quasi-static OLB. Similar to SLB, the test process can also be divided into three stages including the elastic deformation, crack propagation, and final collapse. Because of different mode ratios arising from different loading locations, the load decreases slightly when the initial delamination crack starts to propagate. Comparing Fig. 5c with Fig. 6c, AE signals under OLB are more uniformly distributed at the 63–100 mm location,

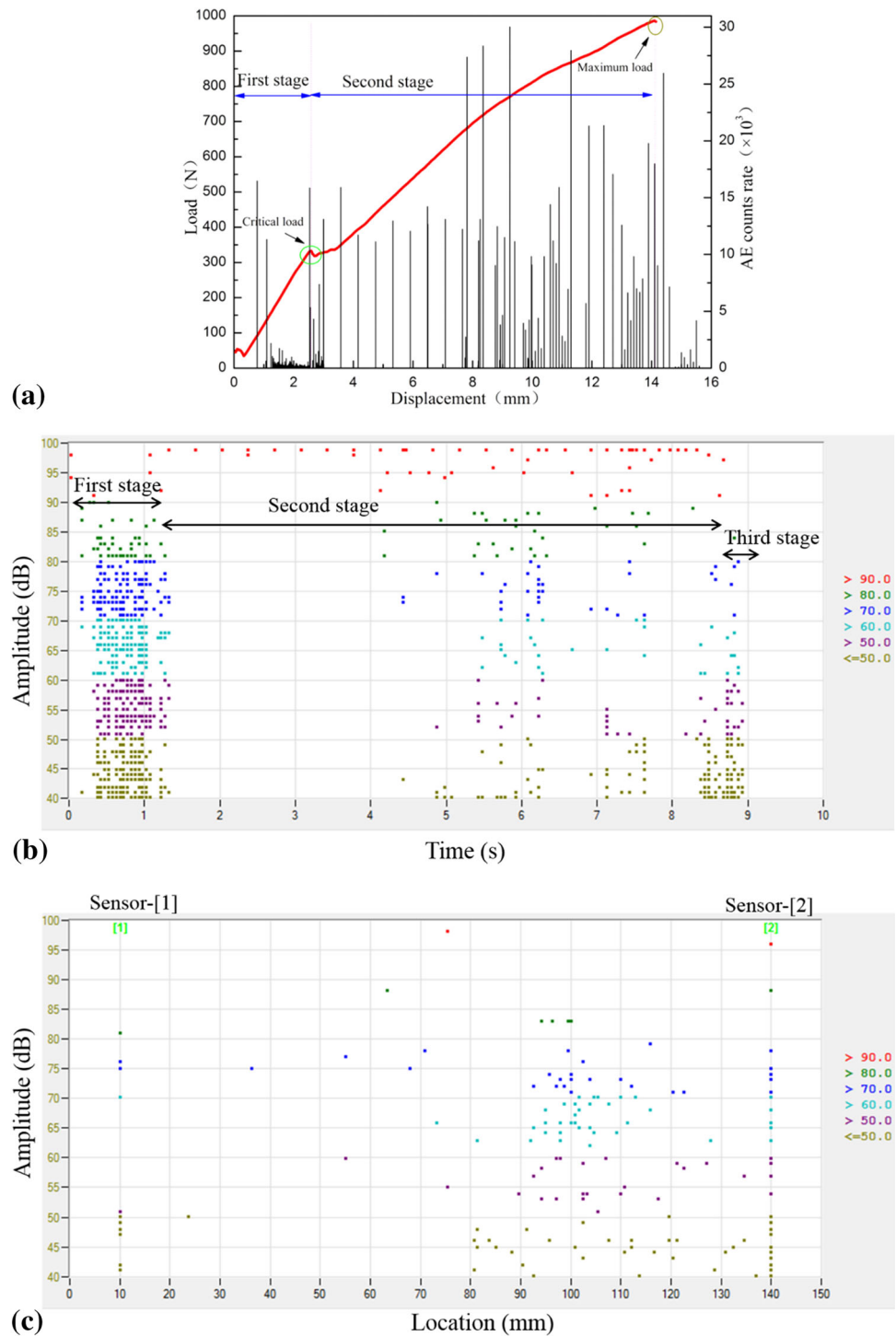
indicating the crack propagation under OLB is more stable [9]. Besides, the crack propagates to the 63 mm location shown in Fig. 6c, shorter than that under SLB.

Delamination Behaviors of Composite Specimens Under Dynamic Loads

Figure 7 shows the load/count rate–displacement distributions, the amplitude–time distribution, and the amplitude–location distribution for the $[0^\circ]_{16}/[0^\circ]_{16}$ specimen under dynamic SLB. The test can be also divided into three stages, similar to the quasi-static loading test above. In the first stage, the amplitude and count rate are higher than those under quasi-static SLB and some fiber breakage signals arise, indicating dynamic impact has a great influence on the specimen in the early test. As shown in Fig. 7a, b, high and sparse count rate is mixed with signals with higher than 80 dB when the crack propagation starts, caused by the fiber breakage which experiences the elastic deformation at the crack tip. Before initial delamination, there is mainly matrix cracking, interface debonding, interlaminar delamination, and a little fiber breakage at the crack tip where fibers still bear the load. When the fiber stress exceeds the limit, the crack starts to propagate with only fiber breakage. As shown in Fig. 8, different failure mechanisms at the crack tip are observed by scanning electron microscope (SEM). In the middle and late periods of the second stage, the AE count rate is more dense with more matrix cracking, interface debonding, and interlaminar delamination signals due to crack propagation. Under dynamic loads, AE signals are fewer than those under quasi-static loads because of higher loading speed. Besides, the number of fiber breakage is higher than that under quasi-static SLB during crack propagation. According to Fig. 7c, the crack propagates to approximately the 85 mm location. The propagation length under dynamic loads is much shorter than that under quasi-static loads.

Figure 9 shows the load/count rate–displacement distributions, the amplitude–time distribution, and the amplitude–location distribution for the $[0^\circ]_{16}/[0^\circ]_{16}$ specimen under dynamic OLB. When the crack starts to propagate under dynamic OLB, the load decreases slightly with sparse count rate and signals with higher than 80 dB, indicating only fiber breakage occurs. As shown in Figs. 9a, b, 10, various failure modes are generated at the crack tip including matrix cracking, interface debonding, delamination which concentrate mainly on the first stage, but fiber breakage appears mainly at the second stage. The AE count rate becomes more dense and higher in the middle and late periods of the second stage due to stable crack propagation and fiber breakage at the loading

Fig. 9 (a) Load/count rate-displacement distributions, (b) amplitude-time distribution, and (c) amplitude-location distribution for the $[0^\circ_{16}/0^\circ_{16}]$ specimen under dynamic OLB



end. According to Fig. 9c, crack propagates to the 90 mm location and the propagation length under dynamic OLB is shorter than that under quasi-static OLB and dynamic SLB.

Figure 11 shows the load/count rate-displacement distributions, the amplitude-time distribution, and the

amplitude-location distribution for the $[0^\circ/90^\circ]_{4s}/[0^\circ/90^\circ]_{4s}$ specimen under dynamic SLB. The test for the $[0^\circ/90^\circ]_{4s}/[0^\circ/90^\circ]_{4s}$ specimen is also divided into three stages, similar to the $[0^\circ]_{16}/[0^\circ]_{16}$ specimen under SLB above. When the load increases to the critical value which is lower

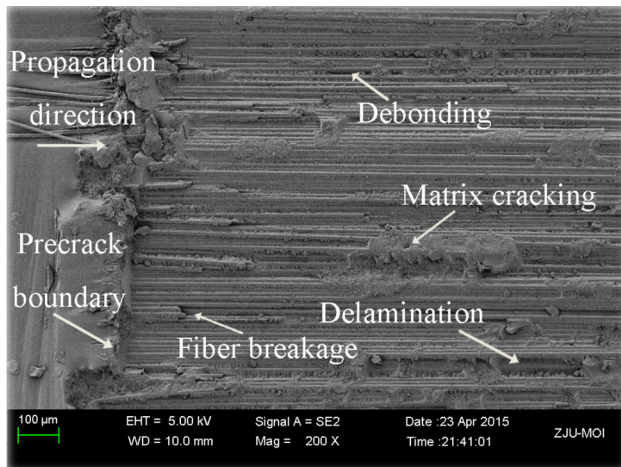


Fig. 10 SEM observation of failure mechanisms at the crack tip for the $[0^\circ]_{16}/[0^\circ]_{16}$ specimen under dynamic OLB

than that for the $[0^\circ]_{16}/[0^\circ]_{16}$ specimen, the delamination crack starts to propagate. This shows the $[0^\circ/90^\circ]_{4s}/[0^\circ/90^\circ]_{4s}$ specimen exhibits weaker delamination resistance under dynamic loads. At the second stage, the AE count rate for the $[0^\circ/90^\circ]_{4s}/[0^\circ/90^\circ]_{4s}$ specimen is higher and more dense than that for the $[0^\circ]_{16}/[0^\circ]_{16}$ specimen because of weaker longitudinal strengths for the $[0^\circ/90^\circ]_{4s}/[0^\circ/90^\circ]_{4s}$ specimen. Besides, there are more signals with all ranges of amplitude, representing more damages during crack propagation. At the final stage, the initial delamination crack propagates completely and high-decibel signals appear at the left location of the specimen, as shown in Fig. 11c.

Figure 12 shows the load/count rate-displacement distributions, the amplitude-time distribution, and the amplitude-location distribution for the $[0^\circ/90^\circ]_{4s}/[0^\circ/90^\circ]_{4s}$ specimen under dynamic OLB. Because of more stable crack propagation under OLB, there is hardly any obvious load decrease when the initial delamination crack starts to propagate. Compared with the $[0^\circ]_{16}/[0^\circ]_{16}$

specimen under dynamic OLB, there are more AE signals with all ranges of amplitude and more dense count rate during crack propagation. At the final delamination stage, the delamination crack propagates completely and high-decibel signals appear at the left location, as shown in Fig. 12c, indicating the delamination resistance for the $[0^\circ/90^\circ]_{4s}/[0^\circ/90^\circ]_{4s}$ specimen is weaker than that for the $[0^\circ]_{16}/[0^\circ]_{16}$ specimen.

Conclusions

This paper originally studies the static and dynamic mixed-mode delamination properties of carbon fiber/epoxy composite laminates under SLB and OLB using AE. By analyzing the response of AE parameters including the amplitude and count rate, the effects of the loading speed, loading mode, and lay-up pattern on the delamination behaviors are explored. From AE test and analysis, three main conclusions are obtained:

1. The evolving delamination crack tip can be judged by identifying the AE amplitude-location distributions. Compared with the $[0^\circ]_{16}/[0^\circ]_{16}$ specimen, the $[0^\circ/90^\circ]_{4s}/[0^\circ/90^\circ]_{4s}$ specimen under dynamic loading experiences more distinct delamination stage represented by more AE amplitude signals and more dense AE count rate.
2. Compared with the $[0^\circ]_{16}/[0^\circ]_{16}$ specimen under quasi-static loading, the $[0^\circ]_{16}/[0^\circ]_{16}$ specimen under dynamic loading exhibits stronger bearing capacity and delamination resistance. However, the $[0^\circ/90^\circ]_{4s}/[0^\circ/90^\circ]_{4s}$ specimen leads to opposite results.
3. The delamination crack propagation is more stable for the OLB loading mode than that for the SLB loading mode, represented by more uniformly distributed amplitude signals for the OLB loading mode than those for the SLB loading mode.

Fig. 11 (a) Load/count rate-displacement distributions, (b) amplitude-time distribution, and (c) amplitude-location distribution for the $[0^\circ/90^\circ]_{4s} //$ $[0^\circ/90^\circ]_{4s}$ specimen under dynamic SLB

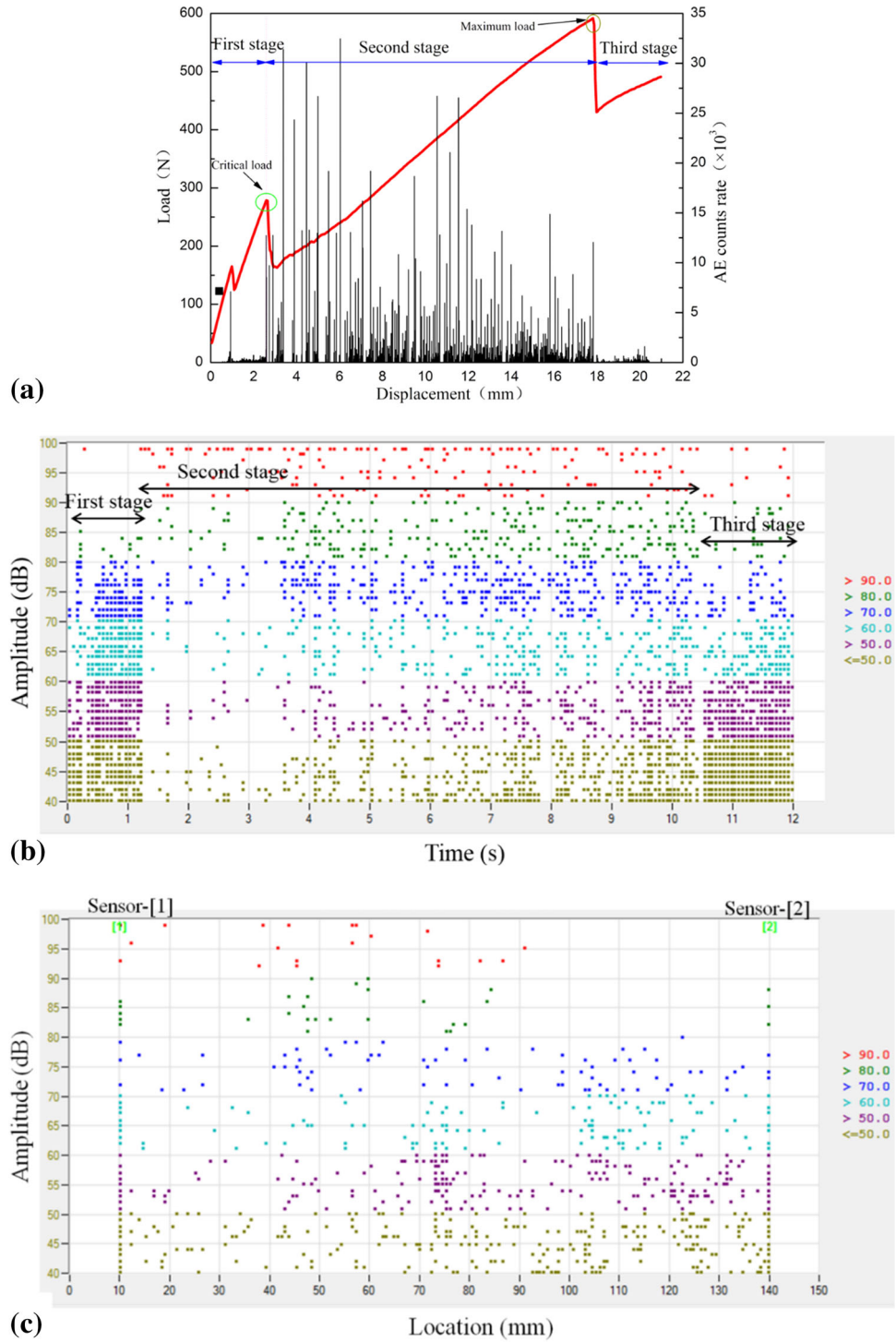
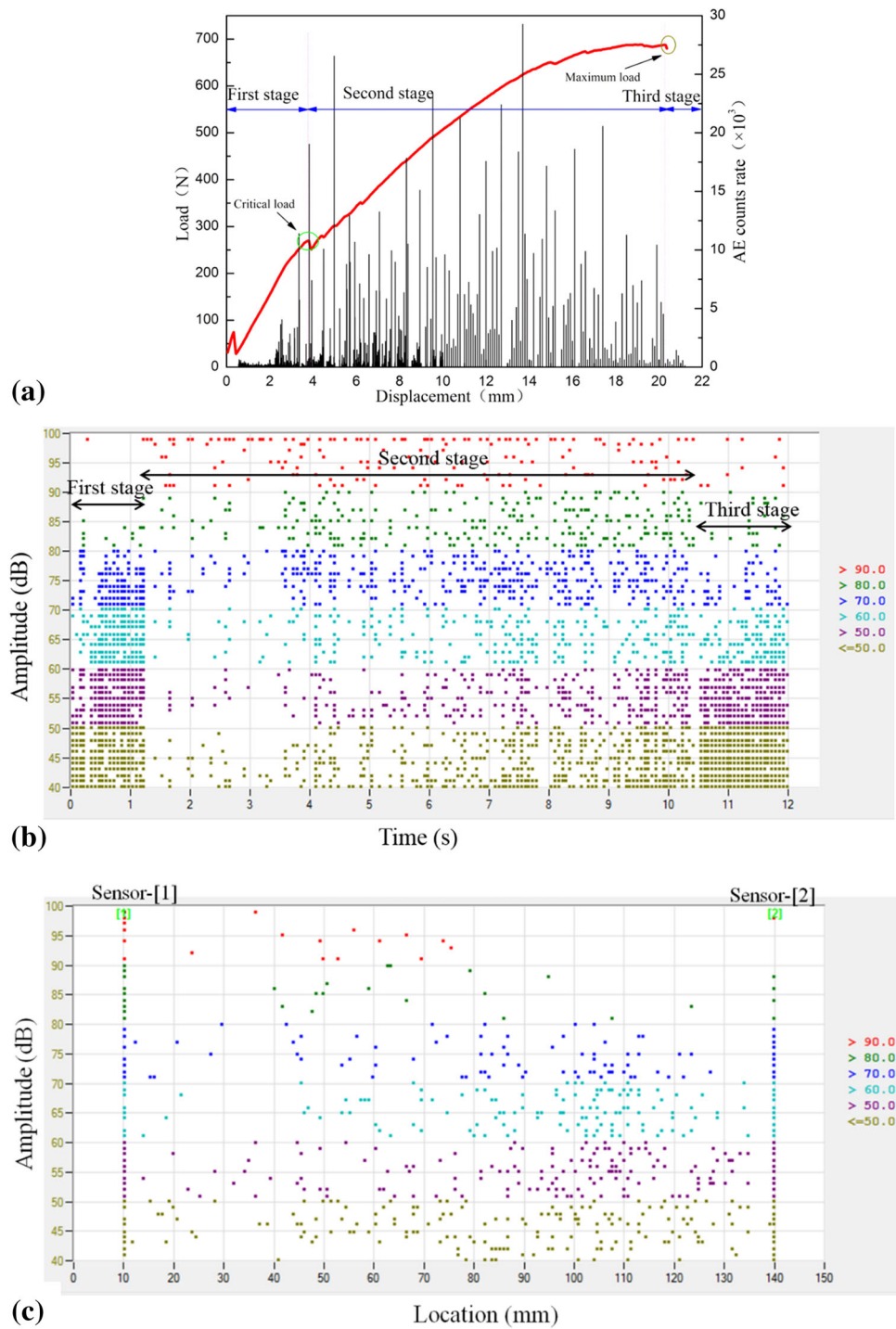


Fig. 12 (a) Load/count rate-displacement distributions, (b) amplitude-time distribution, and (c) amplitude-location distribution for the $[0^\circ/90^\circ]_{4s}/[0^\circ/90^\circ]_{4s}$ specimen under dynamic OLB



Acknowledgments Dr. P.F. Liu would sincerely like to thank the support by the National Natural Science Funding of China (No. 51375435), the National Key Fundamental Research and Development Project (No. 2015CB057603), the Natural Science Funding of Zhejiang Province of China (No. LY13E050002), and Aerospace Science and Technology Innovation Funding.

References

1. F. Dharmawan, G. Simpson, I. Herzberg, S. John, Mixed mode fracture toughness of GFRP composites. *Compos. Struct.* **75**, 328–338 (2006)

2. A.B. Pereira, A.B. de Morais, Mixed mode I + II interlaminar fracture of glass/epoxy multidirectional laminates-Part 2: experiments. *Compos. Sci. Technol.* **66**, 1896–1902 (2006)
3. I.M. De Rosa, C. Santulli, F. Sarasinia, Acoustic emission for monitoring the mechanical behaviour of natural fibre composites: a literature review. *Compos. Part A* **40**, 1456–1469 (2009)
4. K.M. Bak, K. Kalaichelvan, V. Arumugam, A novel approach for classification of failure modes in single lap joints using acoustic emission data. *J. Compos. Mater.* **48**, 3003–3017 (2014)
5. M. Fotouhi, F. Pashmforoush, M. Ahmadi, A.R. Oskouei, Monitoring the initiation and growth of delamination in composite materials using acoustic emission under quasi-static three-point bending test. *Reinf. Plast. Compos.* **30**, 1481–1493 (2011)
6. J.J. Scholey, D.W. Paul, R.W. Michael, Quantitative experimental measurements of matrix cracking and delamination using acoustic emission. *Compos. Part A* **41**(5), 612–623 (2010)
7. I. Silversides, A. Maslouhi, G. LaPlante, Acoustic emission monitoring of interlaminar delamination onset in carbon fiber composites. *Struct. Health Monit.* **12**, 126–140 (2013)
8. P.F. Liu, J. Yang, B. Wang, Z.F. Zhou, J.Y. Zheng, A study on the intralaminar damage and interlaminar delamination of carbon fiber composite laminates under three-point bending using acoustic emission. *J. Fail. Anal. Prev.* **15**(1), 101–121 (2015)
9. A. Szekrenyes, J. Uj, Over-leg bending test for mixed-mode I/II interlaminar fracture in composite laminates. *Int. J. Damage Mech.* **16**(1), 5–33 (2007)
10. A.R. Oskouei, M. Ahmadi, Acoustic emission characteristics of mode I delamination in glass/polyester composites. *J. Compos. Mater.* **44**, 793–807 (2010)
11. X.M. Zhuang, X. Yan, Investigation of damage mechanisms in self-reinforced polyethylene composites by acoustic emission. *Compos. Sci. Technol.* **66**, 444–449 (2006)
12. M. Hajikhani, M. Ahmadi, M. Farjpour, A.R. Oskouei, A. Sharifi, Strain energy release rate assessment in mode I delamination of foam core sandwich composites by acoustic emission. *J. Compos. Mater.* **45**, 2271–2277 (2011)
13. P.F. Liu, J.K. Chu, Y.L. Liu, A study on the failure mechanisms of carbon fiber/epoxy composite laminates using acoustic emission. *Mater. Des.* **37**, 228–235 (2012)
14. V. Arumugam, A.A.P. Sidharth, C. Santulli, Failure modes characterization of impacted carbon fiber reinforced plastics laminates under compression loading using acoustic emission. *J. Compos. Mater.* **48**, 3457–3468 (2014)